

Compact Dual-mode Microstrip Bandpass Filter Based on Greek-cross Fractal Resonator

Hongshu LU, Weiwei WU, Jingjian HUANG, Xiaofa ZHANG, Naichang YUAN

College of Electronic Science and Engineering, National University of Defense Technology, Changsha, Hunan, 410073, China

Luhongshu0321@163.com

Submitted December 14, 2016 / Accepted February 20, 2017

Abstract. *A geometrically symmetrical fractal structure is presented in this paper to provide an alternative approach for the miniaturization design of microstrip bandpass filters (BPFs). The generation process of the geometric geometry is described in detail, and a new fractal resonator called Greek-cross fractal resonator (GCFR) is produced by etching the proposed fractal configuration on the surface of the conventional dual-mode meandered loop resonator. Four microstrip BPFs based on the first four iterations GCFR are modeled and simulated. The simulation results show that with the increase of the number of iterations, the central frequency of the BPF is gradually moving towards the low frequency, which indicates that the proposed fractal resonator has the characteristic of miniaturization. In addition, the parameter optimization and surface current density distribution are also analyzed in order to better understand the performance of the BPF. Finally, a compact dual-mode BPF based on the third iteration GCFR is designed, fabricated and measured. The measurement results are in good agreement with the simulation ones.*

Keywords

Dual-mode, miniaturization, bandpass filter (BPF), fractal geometry, Greek-cross

1. Introduction

Microstrip bandpass filter (BPF) is an indispensable part in the RF front end of various communication systems. It plays a vital role in filtrating the desired signals in the specified frequency band and suppressing the out of band clutter and interference signals. Consequently, the design of microstrip BPFs is always a hot research topic in wireless communication systems. With the progressive development of wireless communication, the demand for microstrip bandpass filter with excellent performance and compact structure becomes more and more urgent [1].

Miniaturization of BPF is one of fundamental requirements in communication systems. Since the dual-mode

resonator was firstly introduced by Wolff [2], the BPFs with dual-mode resonators have been extremely attractive. This is because each dual-mode resonator can be used as a doubly tuned resonant circuit, so the number of resonators required for a given degree of filter is reduced to half, resulting in a compact filter structure [3]. In addition, dual-mode resonators also have advantageous features such as wide passband, low radiation loss, and easy-to-design layout because transmission-line theory and design tools can easily be exploited [4]. In these literatures [5–9], the filters based on the dual-mode resonator are all built by using the coupling between the two degenerate modes, and the two degenerate modes can be excited by introducing a slot along the orthogonal plane or attaching a capacitive patch to the resonator. A pair of crossed slots with unequal widths acted as the perturbation elements had been embedded in a patch resonator [5]. By adjusting the width of the slots, two degenerate modes were excited, and a pair of transmission zeros (TZs) was also generated, which improved the selectivity of the BPF performance. R.Q. Zhang [6] had applied the arc- and radial-oriented slots to bring down the TM_{01} -like mode and to split the TM_{11} -like mode and its degenerate mode, respectively. By using a pair of square etched areas (SEAs) acted as perturbation elements, the dual mode filtering performance had been excited and two TZs located on either side of the passband were clearly observed [7]. The two TZs could effectively improve the stopband rejection, thus avoiding the interference from other communication systems. A novel capacitance loaded square loop resonator (CLSLR) with spurious response suppression and size reduction had been proposed in [8], and the conception of using the inner patch perturbation elements to split the degenerate modes to form two passbands was firstly put forward. In literature [9], the elliptical and linear phase filtering characteristics could be obtained in the first passband by using the perturbation elements in the form of patch or corner cut, respectively.

The term fractal was firstly proposed by Mandelbrot to represent a class of seemingly irregular geometries [10], since then, many fractal geometries have been widely studied and applied in various microwave devices, such as antennas [11–14], frequency selective surfaces (FSSs) [15], and microstrip BPFs [16]. Unlike Euclidean geometry, the

fractal geometry has two essential properties: space-filling and self-similarity. The self-similarity can be used to achieve multi-band characteristics and the space-filling property can be employed for miniaturization design [17]. Yordanov et al. had made a pioneering work in the application of fractal geometry in the design of filters [18]. Based on the investigation of the Cantor fractal geometry, they predicted the fractal could provide a new and promising breakthrough for the design of filters and reflectors. Prior to this, most of the research efforts had been devoted to the application of fractal structure in antennas. Since then, intensive research efforts have been focused on the application of fractal structures in filters. A compact dual-mode T-shape fractal microstrip resonator was proposed in literature [19] and a shorting pin was added to the resonator to excite the degenerate modes in the lower band. By adjusting the size and position of the shorting pin, the proposed resonator could well meet the design requirements. A Minkowski-island-based (MIB) fractal patch resonator was used to design a dual-mode BPF for the applications of wireless local area network (WLAN) [20]. By the perturbation and T-couple / inner-digital coupling, the wide-band and dual-band responses were obtained, respectively. In order to realize the miniaturization of filter and improve the capability of harmonic suppression, the Koch fractal shaped structure was applied to design a compact microstrip BPF [21]. What's more, the Koch fractal electromagnetic bandgap (KFEBG) structures were applied to design improved low-pass filter (LPF) [22]. Juan de Dios Ruiz et al. had designed high-performance BPFs based on the substrate integrated waveguide (SIW) and half mode SIW (HMSIW) with KFEBG patterns etched on the waveguide surface [23]. Moore curve fractal-shaped spiral resonator could provide 49% size reduction as compared to conventional split ring resonators [24], and the BPFs based on the second and third iterations Moore space-filling curve [25] had narrow band frequency responses, high selectivity and blocked harmonics in out-of-band regions. Hilbert-fork resonator [26] was applied to design tri-band bandstop and bandpass filters with excellent performance, small overall sizes, as well as the possibility of independent control of the passbands. Several dual-mode BPFs based on Sierpinski carpet fractal geometry were presented in [27]. With the increase of the number of iterations, both the insertion loss (IL) and fractional bandwidth (FBW) of the BPFs are reduced, and the return loss and the frequency selectivity are improved.

In this paper, a geometrically symmetrical fractal structure is introduced. A new resonator called Greek-cross fractal resonator in this paper is formed by embedding the fractal configuration in the surface of the conventional meandered loop resonator. A dual-mode BPF based on the third iteration GCFR is designed, fabricated and measured. Measurement results show a very close agreement with the simulated ones.

This paper is organized as follows: The generation process and characteristics of the proposed fractal structure are illustrated in Sec. 2 and four dual-mode BPFs based on

the first four iterations GCFR are modeled and studied in Sec. 3. Section 4 provides the simulation and measurement results. The parameters optimization, mode-splitting characteristic and the surface current distribution are also discussed in this section. Finally, a conclusion is drawn in Sec. 5.

2. Generation Process of Greek-cross Fractal Geometry

In the aspects of the applications of fractals in microwave circuits, the most interesting iteration is the one based on the generator. In that case, two components are needed – the initiator and the generator. The initiator is a set of linear segments that comprise a starting shape of a fractal, whilst the generator is an arranged collection of scaled copies of the initiator [28].

The generation process of the Greek-cross fractal geometry is illustrated in Fig. 1. It can be seen that this fractal structure can be generated by using the following steps:

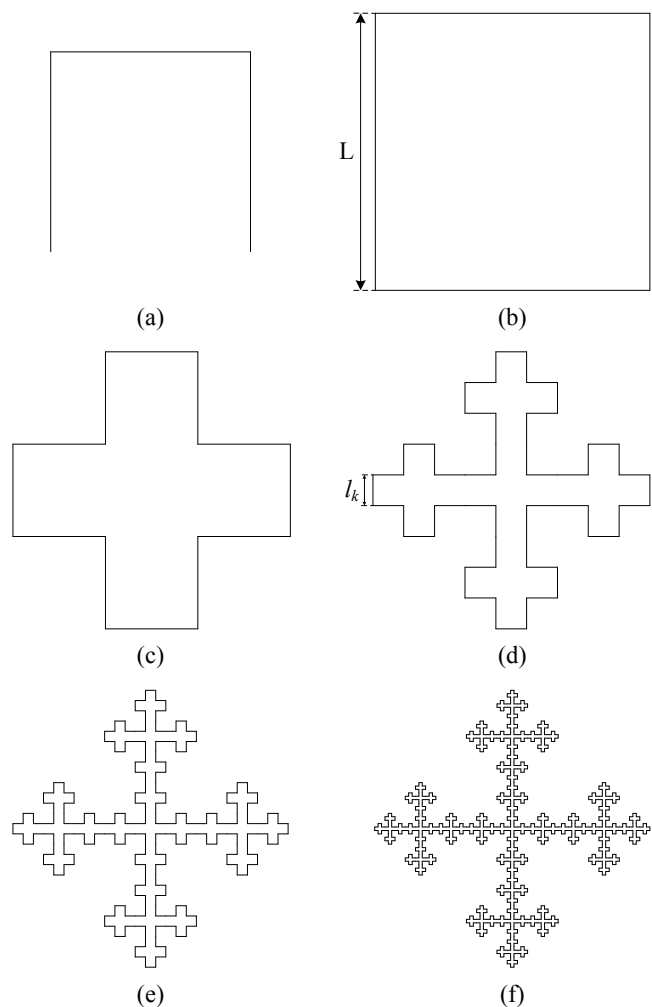


Fig. 1. Generation process of Greek-cross fractal geometry: (a) Generator, (b) Initiator, (c) First iteration, (d) Second iteration, (e) Third iteration, and (f) Fourth iteration.

- The iterative process is started with the initiator, i.e. the zeroth iteration which is a square with the side length of L as shown in Fig. 1(b).
- In the first iteration, each segment of the initiator is replaced by a copy of the generator which is depicted in Fig. 1(a). The dimensions and positions of the copy of the generator are changed so that its end points coincide with the end points of the segment which is to be replaced. Figure 1(c) shows the first iteration of fractal structure.
- In the second iteration, the procedure of copying of the generator is repeated for every segment of the curve obtained after the first iteration. In addition, some line segments which are proportional to the ones of the initiator are added to form a closed curve. Figure 1(d) depicts the second iteration of fractal structure.
- Continuing the above process can obtain the following iterative fractal structures, and the fractal structure of the third and fourth iterations are shown in Fig. 1(e) and Fig. 1(f), respectively.

Theoretically, the iterative process can continue infinitely. However, it has been concluded, in practice, that the number of iterations should be limited to only a few, since otherwise additional complexities arise [29, 30].

The enclosed area donated by A_k of the Greek-cross fractal structure can be derived and given by:

$$A_k = (5/9)^k L^2 \text{ [mm}^2\text{]}, k \geq 0 \quad (1)$$

The perimeter of the Greek-cross fractal structure can be derived and given by:

$$P_k = l_k \times n_k \text{ [mm]}, k \geq 0 \quad (2)$$

$$l_k = 3^{-k} \times L \text{ [mm]}, k \geq 0 \quad (3)$$

$$\left\{ \begin{array}{l} n_0 = 4 \times 1 = 4, k = 0 \\ n_1 = 4 \times 3 = 12, k = 1 \\ n_k = 4 \times \left(3 \times n_{k-1} + 4 \times \sum_{i=0}^{k-2} (3^i \times n_{k-2-i}) \right), k \geq 2 \end{array} \right. \quad (4)$$

where the integer k is the number of iterations, L the side length of the initiator, P_k the perimeter of the fractal geometry after the k -th iteration, n_k the number of the line segments after the k -th iteration, l_k the length of the line segments after the k -th iteration.

From the aspect of miniaturization of circuits, the most important criterion in the selection of a fractal curve is its dimension. The dimension of a fractal curve can be understood as a measure of the space-filling ability of the fractal curve [28]. The higher the fractal dimension, the better the fractal curve fills the given area, therefore achieving higher compactness. The dimension D can be determined as:

$$D = [\log(N)] / [\log(r)] \quad (5)$$

where N is the number of self-similar segments obtained from one segment after each iteration and r is the number of segments obtained from one segment in each iteration. According to Fig. 1, we can obtain $N = 5$ and $r = 3$, therefore, the dimension of the proposed Greek-cross fractal structure can be calculated as $D = 1.465$.

3. Design of Fractal BPF

3.1 Greek-cross Fractal Resonator (GCFR)

A conventional meandered loop resonator as shown in Fig. 2(a) is considered to construct the resonator based on Greek-cross fractal geometry. The reason for this is that the meandered loop resonator can be seen as the first iteration GCFR, which is obtained by etching the first iteration Greek-cross fractal geometry on the surface of a cross-shaped patch. The corresponding iterative fractal resonator can be obtained by etching different iterative fractal geometries on the identical cross-shaped patch. The geometrical structures of fractal resonator based on the first four iterations are depicted in Fig. 2(a) to (d), respectively.

It's obvious that with the increase of the iteration, the surface current path length (the perimeter of the fractal geometry) increases and the width of slot line is reduced. This conclusion can also be verified by (2). Therefore, in

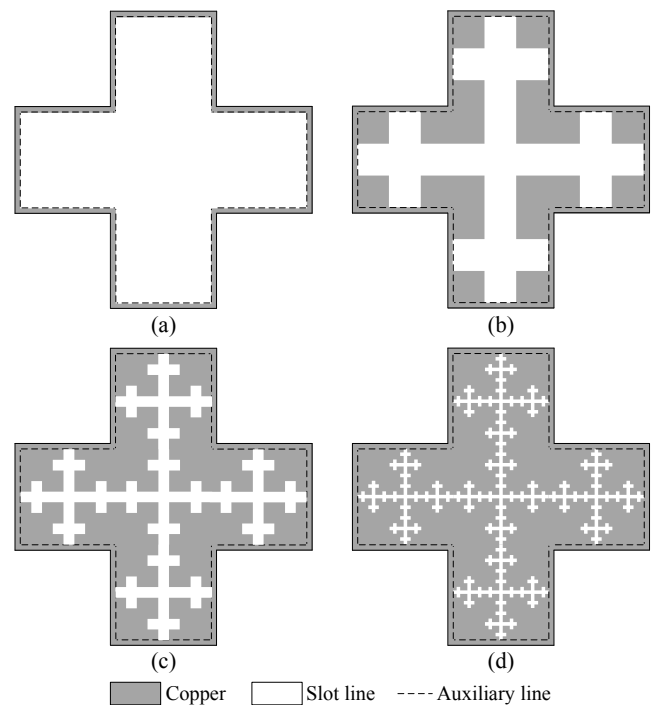


Fig. 2. Geometrical structure of the proposed GCFR based on the first four iterations: (a) First iteration: meandered loop resonator, (b) Second iteration, (c) Third iteration, and (d) Fourth iteration.

the design of the proposed fractal resonator, the main factor that restricts the iterative process is the width of the slot line. More accurately, the main factor that limits the iterative process is the machining precision.

3.2 Characteristics of GCFR

In order to design a BPF based on the proposed fractal resonator with high performance, the fractal resonator should be analyzed firstly. The quality factor Q is an important parameter for the resonant circuit. It can be seen as a measure of the loss of the resonant circuit. In other words, the lower loss means higher Q . In addition, higher Q can also lead to a narrower bandwidth and a more steep response curve. The unloaded quality factor Q_u for the proposed fractal resonator can be obtained from the measurement using the circuit shown in Fig. 3. The Q_u can be calculated by [31]:

$$Q_u = \frac{Q_l}{1 - |S_{21}|}, \quad (6)$$

$$Q_l = \frac{f_{res}}{\Delta f_{3-dB}} \quad (7)$$

where Q_l is the loaded quality factor, S_{21} is the IL at the resonance frequency, f_{res} is the resonance frequency, and Δf_{3-dB} is the 3-dB bandwidth of the f_{res} .

In addition, in the process of measuring the Q_u , it can be observed that with the increase of the number of iterations, the resonance frequency of the resonator is gradually shifted to a lower frequency. Figure 4 shows the effect of the number of iterations on the unloaded quality factor Q_u and normalized resonance frequency ratio R . The R can be found using the following formula:

$$R = \frac{f_{res-k}}{f_{res-1}} \quad (8)$$

where f_{res-k} is the resonance frequency of the k -th iteration resonator and f_{res-1} is the resonance frequency of the first

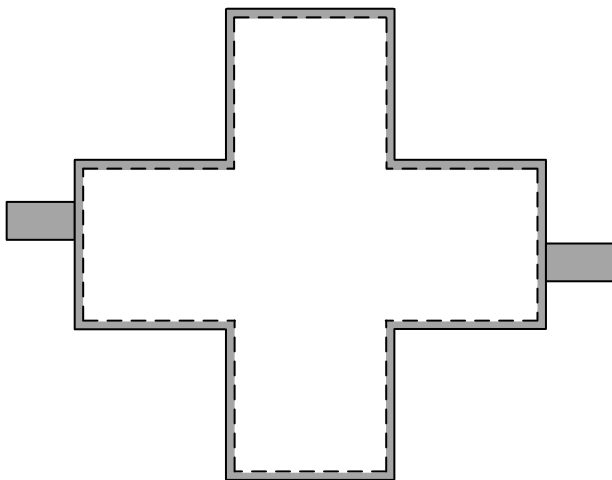


Fig. 3. Sketch map of Greek-cross fractal resonator for the unloaded quality factor Q_u measurement.

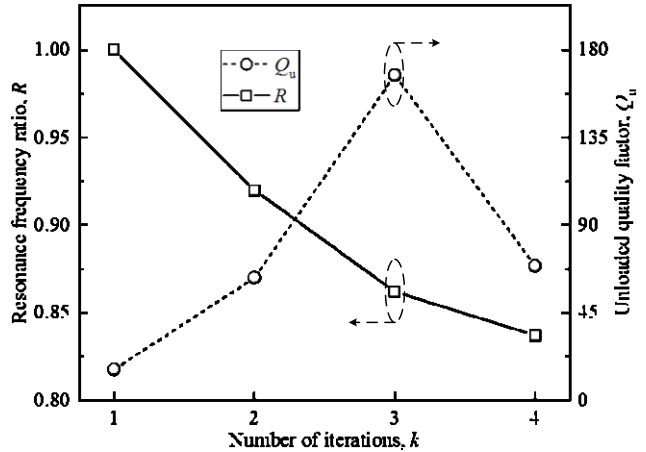


Fig. 4. Normalized resonance frequency ratio R and unloaded quality Q_u against the number k of iterations.

iteration resonator. It can be seen that the change trend gradually becomes more and more slowly with the increase of the number of iteration. So it can be predicted that when k increases to a certain value, R will obtain the minimum value. What's more, the Q_u reaches the maximum value when $k = 3$.

3.3 Filter Design

The geometrical structure of the proposed dual-mode BPF based on the third iteration GCFR is shown in Fig. 5. The other three BPFs are similar in configuration to this one. The only difference is the selected resonator, which is respectively corresponding to the first iteration GCFR, the second iteration GCFR and the fourth iteration GCFR. It has been supposed that these BPFs have been designed on

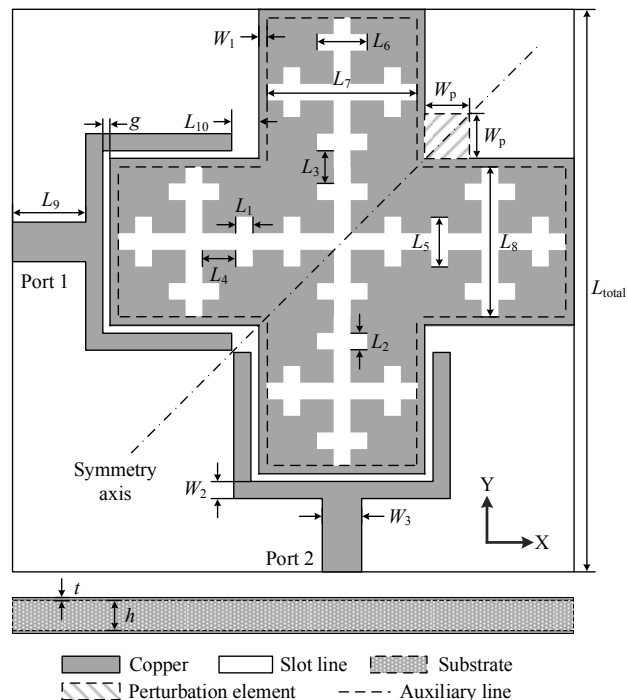


Fig. 5. Geometrical structure of the proposed dual-mode BPF based on the third iteration of GCFR.

the RO3210 substrate with a relative permittivity ϵ_r of 10.8, a thickness h of 1.27 mm and a loss tangent $\tan\delta$ of 0.0027. The thickness t of the copper on the substrate is 35 μm .

The width W_3 of the feed line is chosen to be 0.98 mm, which corresponds to the characteristic impedance of 50 Ω . As depicted in Fig. 5, a pair of orthogonal feed lines as the input and output (I/O) ports are connected to two identical U-shaped coupling arms. The resonator is fed by the U-shaped coupling arms by gap coupling. According to the analysis in [32], the length of the coupling arms and the gap size between the coupling arms and the resonator have a great influence on the performance of the filter. By adjusting the length and the gap size adequately, the coupling strength and the frequency response can be optimized.

It's known that the nature of the coupling between the degenerate modes is an especially significant parameter for dual-mode filter design since it determines the filter characteristics [33]. What's more, the strength and nature of the coupling between the degenerate modes of the dual-mode resonator is mainly determined by the perturbation's size and shape [34]. Therefore, as depicted in Fig. 5, a perturbation element in the form of a small square patch is attached to a corner along the symmetry axis of the GCFR. Of course, the perturbation element can also be other shapes and locations to excite the degenerate modes. However, the manner in this paper is one of the most convenient manners to meet the design requirements. Consequently, the identical perturbation elements are added to the same position of other iterative resonators.

For comparison, the occupied area of the four BPFs is exactly the same, in other words, the length of each BPF donated by L_{total} remains the same. However, in order to obtain better filter performance, the size of some dimensions will be made a fine-tuning, such as L_{10} and W_p , whose variation will not change the value of L_{total} .

4. Performance Evaluation

In this paper, we have investigated the effect of the length of U-shaped coupling arms and the gap size between the coupling arms and the resonator on the performance of the fractal BPF as shown in Fig. 5. Figure 6 and Fig. 7 show the simulation results for five cases from changing the length of the U-shaped coupling arms with a fixed gap size ($g = 0.2$ mm) and varying the gap size with a fixed length ($L_{10} = 0.9$ mm), respectively. It can be seen from Fig. 6(a) that only single mode is excited when L_{10} is less than 0.85 mm. With the increase of L_{10} , the length of the coupling arms is gradually reduced, the two degenerate modes are gradually being excited and moving away from each other. What's more, the reflection characteristic of the BPF is degraded. However, the variation of the length of the coupling arms has little influence on the transmission characteristics of the BPF, which can be evidently concluded from Fig. 6(b). In other words, no matter how the length of the coupling arms changes, the insertion loss in band remains unchanged.

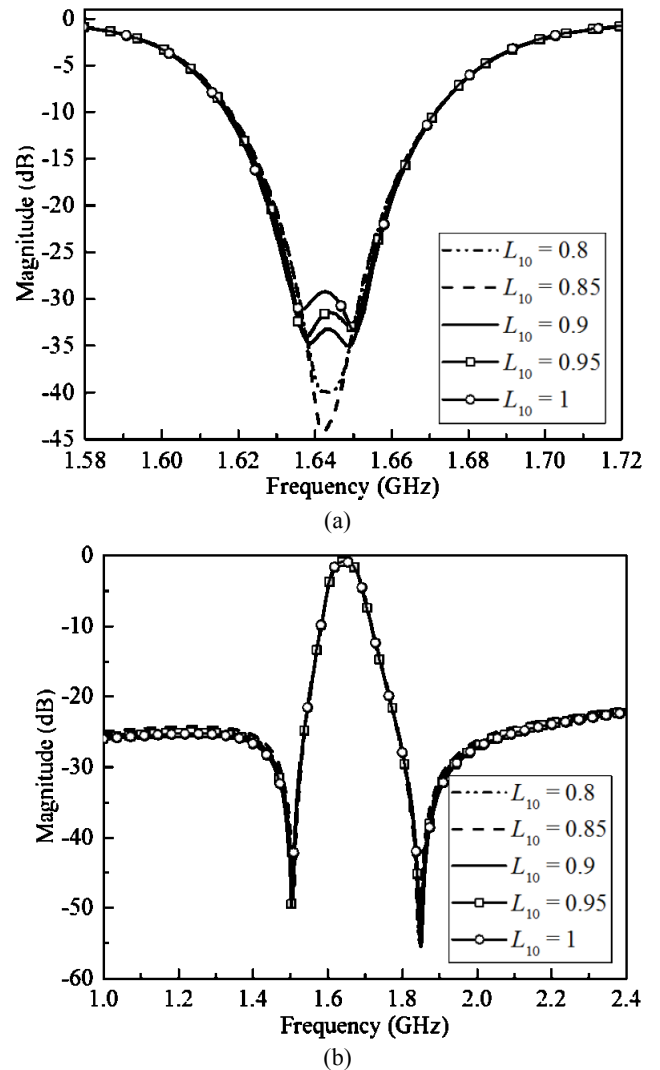


Fig. 6. Simulation results for the performance of the BPF by adjusting the length of the U-shape coupling arms with a fixed gap size ($g = 0.2$ mm). ($W_p = 2.15$ mm) (a) Reflection characteristics (S11). (b) Transmission characteristics (S21).

It's clearly observed from Fig. 7(a) that only single mode is excited when $g = 0.2$ mm, and mode splitting occurs when the value of g is larger than 0.2 mm. With the increase of gap size, the resonance frequencies of the two degenerate modes move away from each other. As shown in Fig. 7(a), higher mode frequency shifts to much higher frequency, while lower mode frequency remains basically constant. As a result, the bandwidth is expanded. The simulation results of the transmission characteristics of the BPF by changing the gap size are shown in Fig. 7(b). Two TZs are located on each side of the passband for these five kinds of conditions. And as the gap size increases, the lower TZs shifts to higher frequency, while the higher TZs shifts to lower frequencies. Combined with the changes in the reflection characteristics mentioned above, it can be concluded that the increase of the gap size can improve the frequency selectivity of the BPF, so that the BPF can obtain sharp passband skirts. Additionally, it's evident from the partial enlarged detail in Fig. 7(b) that with the increase of the gap size g , the single passband gradually splits into

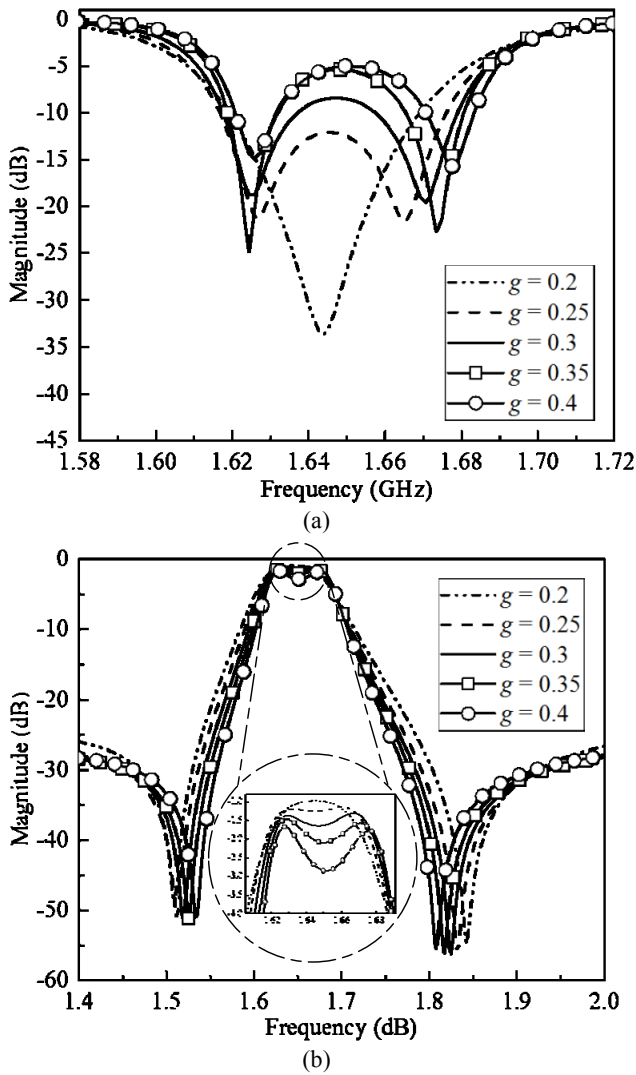


Fig. 7. Simulation results for the performance of the BPF by adjusting the gap size with a fixed length of the U-shape coupling arms ($l_3 = 0.9$ mm), ($W_p = 2.15$ mm): (a) S11, (b) S21.

two frequency bands. The reason for this is that the coupling strength gradually weakens with the increase of the gap size.

In summary, both the length of the coupling arms and the gap size have a certain effect on the characteristics of the BPF. In the design of the BPF, we should focus on the optimization of the two parameters in order to obtain high performance BPF.

Figure 8 shows the simulation results of the change in mode frequencies and coupling coefficient between the degenerate modes with respect to the perturbation size W_p . The coupling coefficient K can be calculated by [35]:

$$K = \frac{f_1^2 - f_2^2}{f_1^2 + f_2^2} \quad (9)$$

where f_1 and f_2 are the resonance frequencies of the mode-I and mode-II, respectively. As it can be seen from Fig. 8, $f_1 = f_2 = 1.644$ GHz and $K = 0$ when $W_p \leq 2.1$ mm. In other words, only single mode is excited and the corresponding

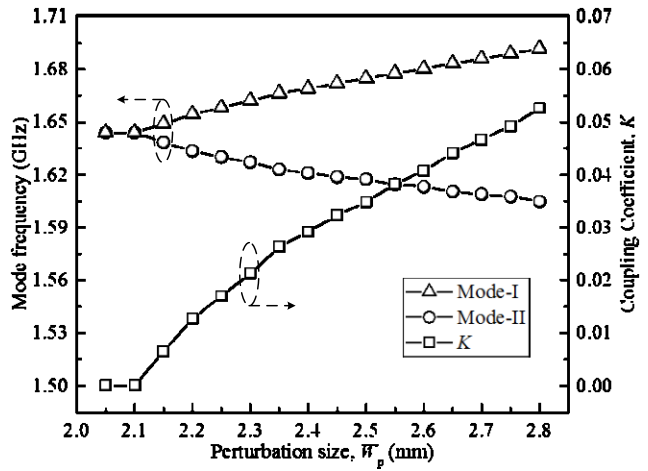


Fig. 8. Simulation results of mode frequency and coupling coefficient between the degenerate modes with respect to the perturbation size W_p ($g = 0.2$ mm, $L_{10} = 0.9$ mm).

coupling coefficient is zero when the perturbation size is less than 2.1 mm. With the increasing of the perturbation size, the two degenerate modes are gradually excited and moving away from each other. It is interesting that the degree of change of the resonance frequencies of the mode-I and mode-II are almost the same. This is because the square perturbation element is symmetrically distributed along the diagonal, and the variation of the perturbation size has the same effect on the electromagnetic field distribution for the mode-I and mode-II. In addition, the coupling coefficient also increases with the increase of the perturbation size.

Based on the above analysis, the physical dimensions of each BPF after optimization are listed in Tab. 1. The simulation results of the frequency responses of these four BPFs are depicted in Fig. 9.

It is obvious from Fig. 9 that all the four fractal BPFs have elliptical frequency responses. In other words, there are two TZs for the passband in the real frequencies. With the increase of the number of iterations, the central frequency of the BPF is shifted to the lower frequency, which is changed from 1.907 GHz in the first iteration to 1.596 GHz in the fourth iteration. Additionally, the corresponding 3-dB bandwidth gradually decreases with the increase of the number of iterations. That is to say, a higher

Dimensions [mm]	First iteration	Second iteration	Third iteration	Fourth iteration
$L_1 = L_2$				0.6
$L_3 = L_4$				1.2
$L_5 = L_6$				1.8
$L_7 = L_8$				5.4
L_9				2
L_{10}	0.9	0.85	0.9	0.8
W_1				0.2
W_2				0.4
W_3				0.98
W_p	2.2	2.2	2.2	2.1
g				0.2
L_{total}				19.2

Tab. 1. Comparison table for different parameters.

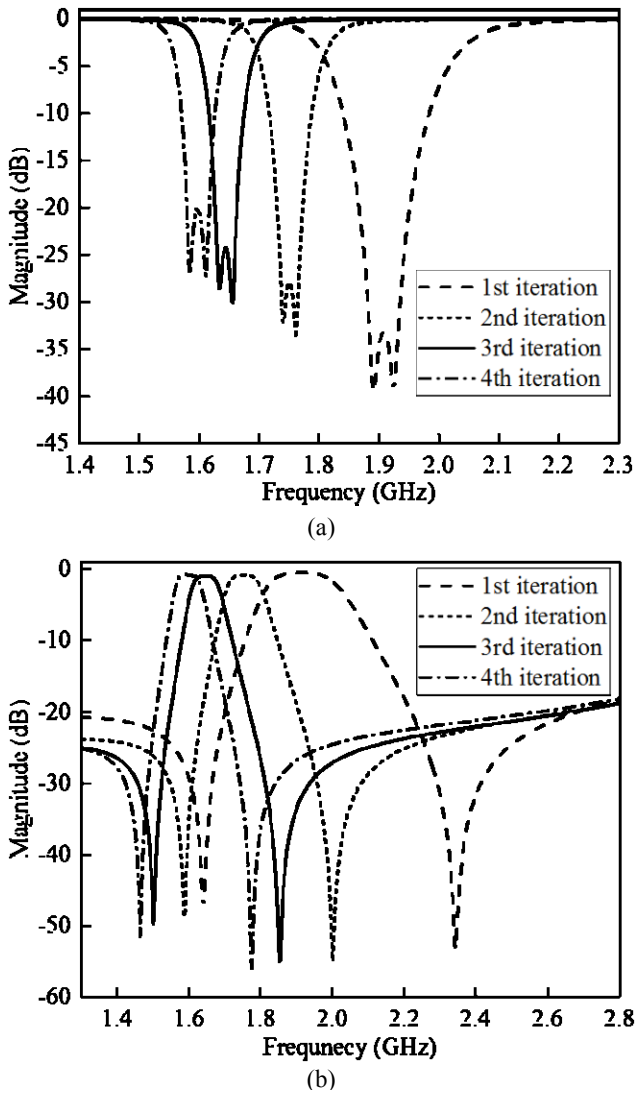


Fig. 9. Simulation results for the frequency responses of the BPF based on GCFRs with different iterations: (a) S11, (b) S21.

iterative BPF can achieve a more steep response curve than the lower one. It can be obtained that the 3-dB bandwidth of these four fractal BPFs is 227 MHz, 111 MHz, 87 MHz and 83 MHz, respectively. Therefore, the corresponding FBW is 11.9%, 6.3%, 5.3% and 5.2%, respectively.

According to the above analysis, a dual-mode BPF based on the third iteration GCFR has been fabricated and measured. The measurement results are achieved by using the Agilent network analyzer PNA-L. The photograph of the fabricated BPF and the simulation and measurement results are illustrated in Fig. 10(a) and (b), respectively. The side length of the BPF is about 20 mm, which is approximate $0.267\lambda_g$, where λ_g is the guided wavelength at the design frequency f_0 . And λ_g can be calculated by the equation [35]:

$$\lambda_g = \frac{c}{f_0 \sqrt{\epsilon_{\text{eff}}}} \quad (10)$$

where c is the speed of light and ϵ_{eff} is the effective dielectric constant, given by [35] as:

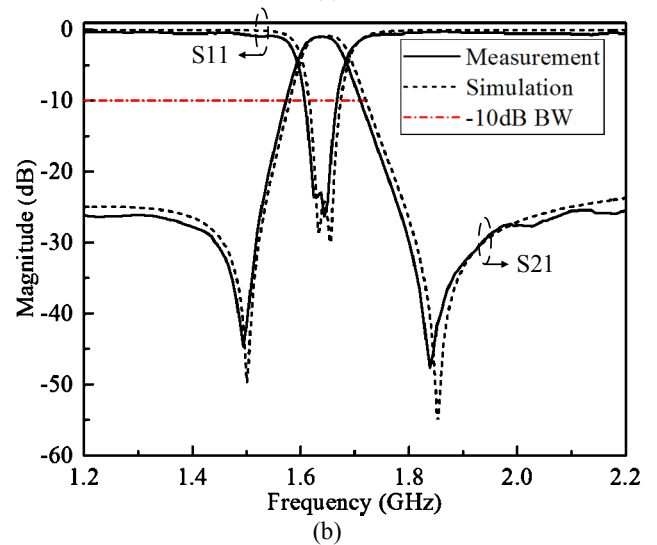
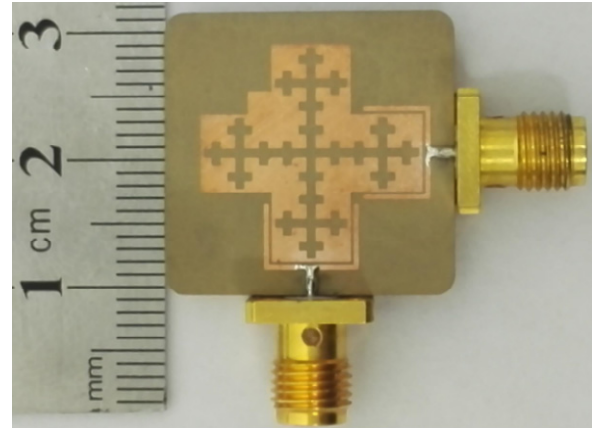


Fig. 10. Final dual-mode BPF based on the third iteration of GCFR. (a) Photograph of the fabricated BPF. (b) Simulation and measurement results for the proposed BPF.

$$\epsilon_{\text{eff}} = \frac{\epsilon_r + 1}{2} \quad (11)$$

where ϵ_r is dielectric constant of the substrate.

As can be seen from Fig. 10(b), the dual-mode BPF operates at the central frequency of 1.65 GHz with a FBW of 5.1%. Two TZs with respective frequency location at 1.507 GHz and 1.851 GHz can be clearly observed. At the lower TZ, the measured S_{21} is about -44.7 dB; while for the higher TZ, the measured S_{21} is about -49.2 dB, and the proposed BPF can effectively suppress harmonic response with a better than 25 dB suppression. Additionally, there are two poles in the passband, and the corresponding frequency and IL are 1.637 GHz with -23.9 dB and 1.656 GHz with -26.5 dB.

In order to get insight into the nature of current density distributions at the surface of the fabricated BPF, the simulation results for the surface current density at four different frequencies of operation are depicted in Fig. 11. In these figures, the maximum current density magnitude indicates the strongest coupling effects while the minimum magnitude indicates the weakest ones. As shown in Figure

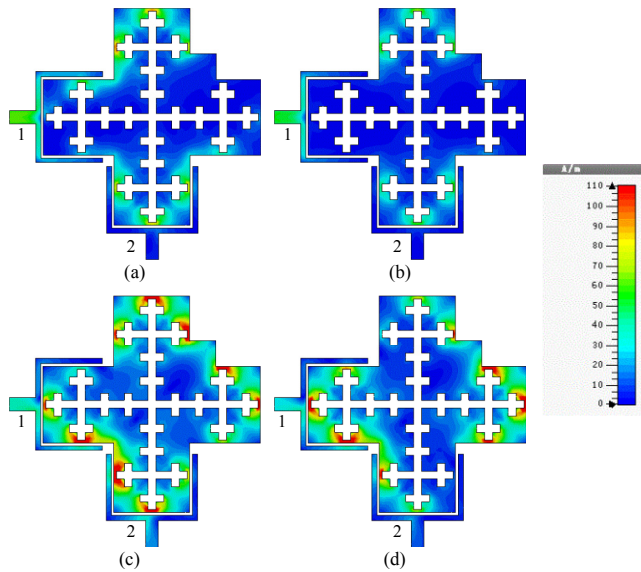


Fig. 11. Simulation results for the current density distribution at the surface on the filter for Port 1: (a) at 1.507 GHz; (b) at 1.851 GHz; (c) at 1.637 GHz; (d) at 1.656 GHz.

11(a) and Fig. 11(b), they are the surface current density distribution of the two TZs at 1.507 GHz and 1.851 GHz, respectively. It's obvious that the energy is mainly distributed on the coupling arm of Port 1 and the upper and lower edges of the resonator, and almost no energy is distributed in the Port 2. This is because the energy is almost reflected back to the Port 1 at the TZs. Figure 11(c) and (d) are the surface current density distribution of the two poles in the passband at 1.637 GHz and 1.656 GHz, respectively. It can be seen that the energy is coupled from Port 1 to Port 2. It's worth noting that the surface current density distributions at 1.637 GHz and 1.656 GHz are different. In addition to the surface current density distribution near the two ports, the energy for 1.637 GHz is mainly distributed on the upper edge of the resonator, while the energy for 1.656 GHz is mainly distributed on the right edge of the resonator. This is because resonance frequencies of two degenerate modes in a resonator have a 90° phase offset, which is the same as their current distributions.

5. Conclusions

In this paper, a compact dual-mode BPF based on the third iteration GCFR is presented. The new fractal resonator has the property of miniaturization in the design of microstrip BPFs. In addition, the generation process of the fractal structure is described in detail. After parameters optimization, a dual-mode BPF operating at 1.65 GHz with a FBW of 5.1% has been designed, fabricated and measured. The measurement results are in a close agreement with the simulation ones. In addition to the machining accuracy, the deviation between the dielectric constant of the substrate and the theoretical value, which is not considered in the simulation, leads to the small deviation between simulation and measurements. Therefore, the proposed fractal resonator can be used in the miniaturized design of

microwave components in modern satellite and wireless communication systems.

Acknowledgments

This work is supported by the National Science Foundation of China under Grant No.61302017. The authors would like to thank the editor, the associate editor, and the anonymous reviewers for their valuable comments and suggestions that greatly improved this paper.

References

- [1] NAGHAR, A., AGHZOUT, O., ALEJOS, A.V., et al. Design of compact multiband bandpass filter with suppression of second harmonic spurious by coupling gap reduction. *Journal of Electromagnetic Waves and Applications*, 2015, vol. 29, no. 14, p. 1813–1828. DOI: 10.1080/09205071.2015.1043029
- [2] WOLFF, I. Microstrip bandpass filter using degenerate modes of a microstrip ring resonator. *Electronic Letters*, 1972, vol. 8, no. 12, p. 302–303. DOI: 10.1049/el:19720223
- [3] WANG, J.-P., WANG, L., GUO, Y.-X., et al. Miniaturized dual mode bandpass filter with controllable harmonic response for dual band applications. *Journal of Electromagnetic Waves and Applications*, 2009, vol. 23, no. p. 1525–1533. DOI: 10.1163/156939309789476482
- [4] ZHU, L., WECOWSKI, P.-M., WU, K. New planar dual-mode filter using cross-slotted patch resonator for simultaneous size and loss reduction. *IEEE Transactions on Microwave Theory and Techniques*, 1999, vol. 47, no. 5, p. 650–654. DOI: 10.1109/22.763171
- [5] WU, S., WENG, M.-H., JHONG, S.-B., et al. A novel crossed slotted patch dual-mode bandpass filter with two transmission zeros. *Microwave and Optical Technology Letters*, 2008, vol. 50, no. 3, p. 741–744. DOI: 10.1002/mop.23219
- [6] ZHANG, R., ZHU, L., LUO, S. Dual-mode dual-band bandpass filter using a single slotted circular patch resonator. *IEEE Microwave and Wireless Components Letters*, 2012, vol. 22, no. 5, p. 233–235. DOI: 10.1109/lmwc.2012.2192419
- [7] SU, Y.-K., CHEN, J.-R., WENG, M.-H., et al. Design of a miniature and harmonic control patch dual-mode bandpass filter with transmission zeros. *Microwave and Optical Technology Letters*, 2008, vol. 50, no. 8, p. 2161–2163. DOI: 10.1002/mop.23604
- [8] FU, S., WU, B., CHEN, J., et al. Novel second-order dual-mode dual-band filters using capacitance loaded square loop resonator. *IEEE Transactions on Microwave Theory and Techniques*, 2012, vol. 60, no. 3, p. 477–483. DOI: 10.1109/tmtt.2011.2181859
- [9] KARPUZ, C., GORUR, A.K., SAHIN, E. Dual-mode dual-band microstrip bandpass filter with controllable center frequency. *Microwave and Optical Technology Letters*, 2015, vol. 57, no. 3, p. 639–642. DOI: 10.1002/mop.28914
- [10] MANDELBROT, B. B. *The Fractal Geometry of Nature*. 1st ed., New York (USA): W. H. Freeman and Company, 1983. ISBN: 0716711869
- [11] SONG, C.T.P., HALL, P.S., GHAFOURI-SHIRAZ, H., WAKE, D. Sierpinski monopole antenna with controlled band spacing and input impedance. *Electronic Letters*, 1999, vol. 36, no. 13, p. 1036 to 1037. DOI: 10.1049/el:19990748

- [12] PUENTE, C., ANGUERA, J., BORJA, C., et al. Fractal-shaped antennas and their application to GSM 900/1800. *The Journal of the Institution of British Telecommunication Engineers*, 2001, vol. 2, no. 3, p. 92–95.
- [13] ANGUERA, J., PUENTE, C., BORJA, C., et al. Fractal-shaped antennas: A review. *Encyclopedia of RF and Microwave Engineering*, 2005, vol. 2, p. 1620–1635. DOI: 10.1002/0471654507.eme128
- [14] ANGUERA, J., DANIEL, J. P., BORJA, C., et al. Metallized foams for antenna design: application to fractal-shaped Sierpinski-carpet monopole. *Progress in Electromagnetics Research*, 2010, vol. 104, p. 239–251. DOI: 10.2528/pier10032003
- [15] WERNER, D. H., LEE, D. Design of dual-polarized multiband frequency selective surfaces using fractal elements. *Electronic Letters*, 2000, vol. 36, no. 6, p. 487–488. DOI: 10.1049/el:20000457
- [16] NEETHU, S., SANTHOSH KUMAR, S. Microstrip bandpass filter using fractal based hexagonal loop resonator. In *2014 Fourth International Conference on Advances in Computing and Communications (ICACC 2014)*. Kochi (India), 2014, p. 319–322. DOI: 10.1109/ICACC.2014.81
- [17] ORIZI, H., SOLEIMANI, H. Miniaturisation of the triangular patch antenna by the novel dual-reverse-arrow fractal. *IET Microwaves, Antennas and Propagation*, 2015, vol. 9, no. 7, p. 627–633. DOI: 10.1049/iet-map.2014.0462
- [18] YORDANOV, O. I., ANGELOV, I., KONOTOP, V. V., et al. Prospects of fractal filters and reflectors. In *1991 Seventh International Conference on (IEE) Antennas and Propagation (ICAP 91)*. New York (USA), 1991, p. 698–700.
- [19] AHMED, E. S. Dual-mode dual-band microstrip bandpass filter based on fourth iteration T-square fractal and shorting pin. *Radioengineering*, 2012, vol. 21, no. 2, p. 617–623.
- [20] LIU, J.-C., CHANG, C. C., KUEI, C.-P., et al. Dual-mode wide-band and dual-band resonators with Minkowski-island-based fractal patch for WLAN systems. In *Cross Strait Quad-Regional Radio Science and Wireless Technology Conference (CSQRWC 2011)*. Harbin (Heilongjiang, China), 2011, p. 583–585. DOI: 10.1109/CSQRWC.2011.6037017
- [21] ESA, M., THAYAPARAN, D., ABDULLAH, M. S., et al. Miniaturized microwave modified Koch fractal hairpin filter with harmonic suppression. In *2010 IEEE Asia-Pacific Conference on Applied Electromagnetics (APACE 2010)*. Port Dickson (Negeri Sembilan, Malaysia), Malaysia, 2010, p. 1–4. DOI: 10.1109/APACE.2010.5719750
- [22] de DIOS-RUIZ, J., MARTÍNEZ-VIVIENTE, F. L., HINOJOSA, J. Optimisation of chirped and tapered microstrip Koch fractal electromagnetic bandgap structures for improved low-pass filter design. *IET Microwaves, Antennas and Propagation*, 2015, vol. 9, no. 9, p. 889–897. DOI: 10.1049/iet-map.2014.0453
- [23] de DIOS-RUIZ, J., MARTINEZ-VIVIENTE, F. L., ALVAREZ-MELCON, A., et al. Substrate integrated waveguide (SIW) with Koch fractal electromagnetic bandgap structures (KFEBG) for bandpass filter design. *IEEE Microwave and Wireless Components Letters*, 2016, vol. 25, no. 3, p. 160–162. DOI: 10.1109/LMWC.2015.2390537
- [24] GHATAK, R., PAL, M., GOSWAMI, C., et al. Moore curve fractal-shaped miniaturized complementary spiral resonator. *Microwave and Optical Technology Letters*, 2013, vol. 55, no. 8, p. 1950–1954. DOI: 10.1002/mop.27682
- [25] MEZAAL, Y. S., ALI, J. K., EYYUBOGLU, H. T. Miniaturised microstrip bandpass filters based on Moore fractal geometry. *International Journal of Electronics*, 2015, vol. 102, no. 8, p. 1306–1319. DOI: 10.1080/00207217.2014.971351
- [26] JANKOVIC, N., GESCHKE, R., CRNOJEVIC-BENGIN, V. Compact tri-band bandpass and bandstop filters based on Hilbert-Fork resonators. *IEEE Microwave and Wireless Components Letters*, 2013, vol. 23, no. 6, p. 282–284. DOI: 10.1109/LMWC.2013.2258005
- [27] SONI, V., KUMAR, M. New kinds of fractal iterated and miniaturized narrowband bandpass filters for wireless applications. In *2014 International Conference on Advances in Computing Communications and Informatics (ICACCI 2014)*. Delhi (India), 2014, p. 2786–2792. DOI: 10.1109/ICACCI.2014.6968632
- [28] CRNOJEVIC-BENGIN, V. *Advances in Multi-Band Microstrip Filters*. 1st ed. United Kingdom: Cambridge University Press, 2015. ISBN: 978-1-107-08197-0
- [29] FALCONER, K. *Fractal Geometry: Mathematical Foundations and Applications*. 1st ed. Chichester (UK): John Wiley and Sons Ltd., ISBN: 2003. 0-470-84861-8
- [30] PEITGEN, H.-O., JURGENS, H., SAUPE, D. *Chaos and Fractals*. 1st ed. New York (USA): Springer-Verlag, 2004. ISBN: 978-1-4684-9396-2
- [31] YE, C.S., SU, Y.K., WENG, M.H., et al. Resonant properties of the Sierpinski-based fractal resonator and its application on low-loss miniaturized dual-mode bandpass filter. *Microwave and Optical Technology Letters*, 2009, vol. 51, no. 5, p. 1358–1361. DOI: 10.1002/mop.24321
- [32] HSIEH, L.-H., CHANG, K. Dual-mode quasi-elliptic-function bandpass filters using ring resonators with enhanced-coupling tuning stubs. *IEEE Transaction on Microwave Theory and Techniques*, 2002, vol. 50, no. 5, p. 1340–1345. DOI: 10.1109/22.999148
- [33] GORUR, A. Description of coupling between degenerate modes of a dual-mode microstrip loop resonator using a novel perturbation arrangement and its dual-mode bandpass filter applications. *IEEE Transactions on Microwave Theory and Techniques*, 2004, vol. 52, no. 2, p. 671–677. DOI: 10.1109/TMTT.2003.822033
- [34] MANSOUR, R. R. Design of superconductive multiplexers using single-mode and dual-mode filters. *IEEE Transactions on Microwave Theory and Techniques*, 1994, vol. 42, no. 7, p. 1411 to 1418. DOI: 10.1109/22.299738
- [35] HONG, J.-S., LANCASTER, M. J. *Microstrip Filters for RF/Microwave Applications*. 1st ed. New York (USA): John Wiley and Sons Ltd., 2001. ISBN: 0-471-38877-7

About the Authors ...

Hongshu LU was born in 1988. He received his M.S. degree in Electronic Science and Technology from the National University of Defense Technology in 2013. Currently he is working towards the Ph.D. degree in the College of Electronic Science and Engineering, National University of Defense Technology, Changsha, Hunan, China. His research interests include passive microwave circuits design and wireless communication.

Weimei WU was born in 1981. She received her M.S. and Ph.D. degree in Electronic Science and Technology from the National University of Defense Technology in 2008 and 2011, respectively. Currently she is a teacher in the College of Electronic Science and Engineering, National University of Defense Technology, Changsha, Hunan,

China. Her research interests include antennas design and wave propagation.

Jingjian HUANG was born in 1983. He received his Ph.D. degree in Electronic Science and Technology from the National University of Defense Technology in 2014. Currently he is a teacher in the College of Electronic Science and Engineering, National University of Defense Technology, Changsha, Hunan, China. His research interests include antennas design and wave propagation.

Xiaofa ZHANG was born in 1978. He received his Ph.D. degree in Electronic Science and Technology from the National University of Defense Technology in 2007.

Currently he is a teacher in the College of Electronic Science and Engineering, National University of Defense Technology, Changsha, Hunan, China. His research interests include microwave circuits and antennas design.

Naichang YUAN was born in 1965. He received his M.S. and Ph.D. degree in Electronic Science and Technology from the University Science and Technology of China in 1991 and 1994, respectively. He is currently a professor with the College of Electronic Science and Engineering, National University of Defense Technology, Changsha, Hunan, China. His research interests include microwave circuits design, wireless communication, antennas and wave propagation.